Pushing electrons in one dimension

Candidate 8238X[†]

[†] Cavendish Laboratory, Cambridge University, JJ Thomson Avenue, Cambridge, CB3 0HE, UK

Abstract. We consider the effect of 'shunts' on an ultracold 1D gas of fermions confined to an infinite square well - diabatic quenches where the well instantly acquires a constant velocity. In the absence of interactions an analytic approach is developed to characterise the solutions for shunts both subsonic and hypersonic with respect to the Fermi-velocity. We further consider the case of Coulomb-interactions in a physical quasi-1D gas with a radial harmonic transverse confinement. The Hartree-Fock formalism admits an exact solution for the exchange potential, similar to that of 3D jellum. Time-Dependent Hartree-Fock Theory (TDHFT) is implemented to study the phenomenology of shunts in the physical gas.

Keywords: quasi-one-dimensional, jellium, Fermi-gas, quantum shock, quantum sound, Hartree-Fock

Submitted to: *[assessment version]*

1. Introduction

There is a considerable body of experimental and theoretical work[3] on the effects of radiation on metallic crystals at the level of the crystal structure (i.e. in terms of the arrangement of the ions): phenomena such as embrittlement and foaming may be attributed to the formation of defects, voids, dislocation pinning, etc. However these permanent phenomena must be the result of processes acting over much shorter timescales. When a particle of radiation traverses a metallic crystal, it loses energy to both the ions and the delocalised electrons at a rate with respect to the path length known as the 'stopping power', which typically displays a 'Bragg peak' immediately before the particle is arrested. The radiation damage to the crystal structure arises

partly from the subsequent equilibration of the electrons and ions, through electron-phonon interaction. Hence, an understanding of the effect of the particle on the electrons is necessary for a general understanding of radiation damage. Previous work has focussed on the dynamics of the ions in the Born-Oppenheimer approximation[4], where electron state evolution is adiabatic. Many more recent studies[5], [7], [8] have applied Time Dependent Density Functional Theory (TDDFT) to the electron states. In most metals, the Fermi-velocity is $v_F \approx 10^8$ cm s^{-1}. This may be comparable to the velocity of an α particle, but far below the velocities of β particles or the various charged particles associated with cosmic rays. In these so-called *swift* particles the formation of bow shocks and wakes in the electron gas is anticipated; [6] examines these phenomena in the case of swift molecular ions.

There now exists a very rich selection of formalisms for modelling the weakly perturbed interacting Fermi-gas. The theoretical starting point is generally considered to be Landau's Fermi Liquid Theory, or its counterpart in one dimension, Luttinger Liquid Theory. In computational physics it has become practical to employ dielectric response and TDDFT. Less prevalent in recent years has been the use of Hartree-Fock theory, a mainstay of computational chemistry which can be usefully applied to model homogeneous many-body systems with large particle number, such as electron gases. Time Dependent Hartree-Fock Theory (TDHFT) is a possible candidate for modelling fast, ionizing radiation amongst electrons partly because is not a perturbative method.

We will consider the minimal case of a swift but non-relativistic particle violently impinging on a one-dimensional Fermi-gas. We model this by preparing the gas in the ground state of an infinite square well, and then causing the well to suddenly move at a constant speed - we refer to this as a *shunt*. Such a sudden change in the Hamiltonian of a quantum system is generally known as a *quench*. We will use the words 'quench' and 'shunt' interchangeably. This approach has the advantage that it is general in the shunt speed: it can be applied to non-swift particles. Whilst the 'pushed' end of the well is more relatable to the radiation problem, we will be able to study contrary effects at the 'pulled' end for free (this may, at a pinch, be interpreted as a kind of 'wake' in one dimension).

Beginning in Section 2 with non-interacting Fermions, we will be able to understand the behaviour of the shunted gas to a high degree by merely solving the Schrödinger equation and following the distribution of number density in the well. In Section 3, which may be read independently, we try to make the transition to a *physical* gas. In particular we consider the quantum wire in which the transverse confinement

is a radial harmonic potential. Within Hartree-Fock theory, the 'blurred' form of the Coulomb interactions in the wire leads to an exact solution for the exchange potential; the properties that follow from this may be of interest to experimentalists studying quasi-one-dimensional Fermion gases. Finally in Section 4 we implement TDHFT in a limited study of shunt phenomenology on a length of the quantum wire introduced in Section 3.

Unless otherwise stated, we will work in either natural ($\hbar = 1$, c should not arise) or CGS-Gaussian units, as is convenient.

2. Non-interacting Fermi-gas

2.1. The quench projection operator

The electrons in a one-dimensional metallic crystal are modelled as a Fermi-gas confined to an infinite square well of length l_0, corresponding to irresistible but homogeneous ionic potentials. The Coulomb interactions are initially neglected. The spatial energy eigenstates within the well can be written $\phi_n = \sqrt{2/l_0}\sin(n\pi x/l_0)$, where the quantum number n indexes the energy spectrum in the usual way. Such a gas containing N Fermions will have average number density N/l_0, but this will not be uniform: as illustrated in figure 1 it will exhibit oscillations dominated by the Fermi-wavelength near the walls of the potential. These are known as *Friedel oscillations.*

From some prepared state we diabatically quench to an identical well which moves at velocity v from the initial position. Inside the moving well, in the original ('laboratory') frame, the new energy eigenstates are,

$$\psi_n = \sqrt{\frac{2}{l_0}} e^{-i\mathcal{E}_n t + imvx} \sin\left(\frac{n\pi\,(x - vt)}{l_0}\right), \quad \mathcal{E}_n = \frac{1}{2}mv^2 + \frac{n^2\pi^2}{2ml_0^2}, \tag{1}$$

as may be confirmed by positing the form,

$$\psi_n \sim f\,(x,t)\sin\left(n\pi\,(x - vt)\,/l_0\right), \tag{2}$$

and solving the Schrödinger equation for $f(x,t)$. The additional phase factor, $\exp(imvx)$, is due to the extra momentum granted to the particle by the motion of the well, and is a general feature of Galilean transformations of the wavefunction. It is convenient to discuss this momentum in terms of the dimensionless number $q = mvl_0/\pi$, to be interpreted in the same sense as n with the caveat that q is

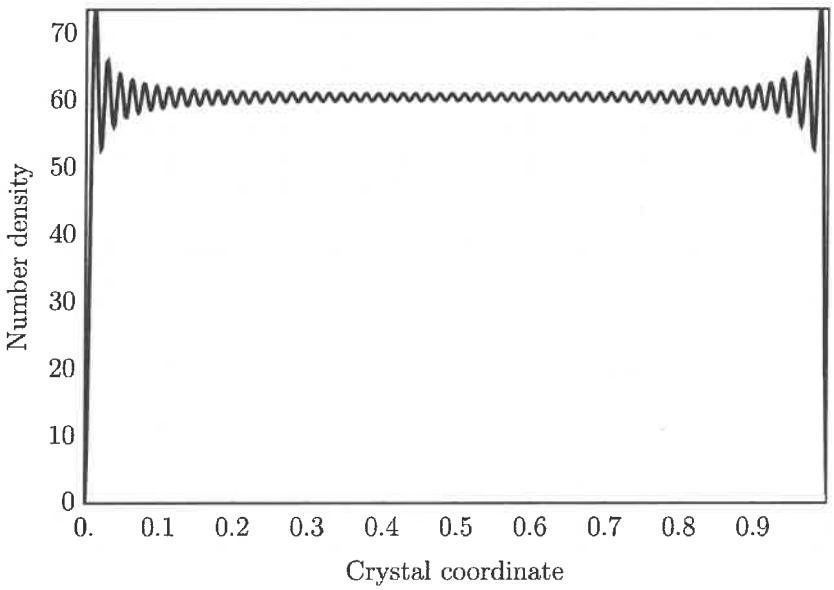

Figure 1. The $N = 60$ Fermi gas exhibiting Friedel oscillations near to the edge of the well. Homogeneity increases towards the well centre.

not strictly a quantum number (indeed, it need not even be an integer). Understood this way, q completely characterises the quench. We are concerned with the unitary projection operator, $\hat{C} = \mathsf{C}_{jk} |\psi_j\rangle \langle\phi_k|$, that effectively carries us between inertial reference frames. The matrix elements have the form,

$$\mathsf{C}_{jk} = -\frac{q\left[1 - e^{-i\pi q}\cos\left(\pi\left(k+j\right)\right) - i\frac{(k+j)}{q}e^{-i\pi q}\sin\left(\pi\left(k+j\right)\right)\right]}{\pi\left(q^2 - \left(k+j\right)^2\right)} + \frac{q\left[1 - e^{-i\pi q}\cos\left(\pi\left(k-j\right)\right) - i\frac{(k-j)}{q}e^{-i\pi q}\sin\left(\pi\left(k-j\right)\right)\right]}{\pi\left(q^2 - \left(k-j\right)^2\right)}, \quad (3)$$

from which we see that C is symmetric, with power concentrated in the elements for which the denominators in (3) are small. An example C is shown in figure 2.

2.2. A formalism for finding the quenched single particle state

In the absence of interactions we can in principle understand the effect of a quench on the gas as a whole by elucidating the effect on ψ_n and summing relevant quantities

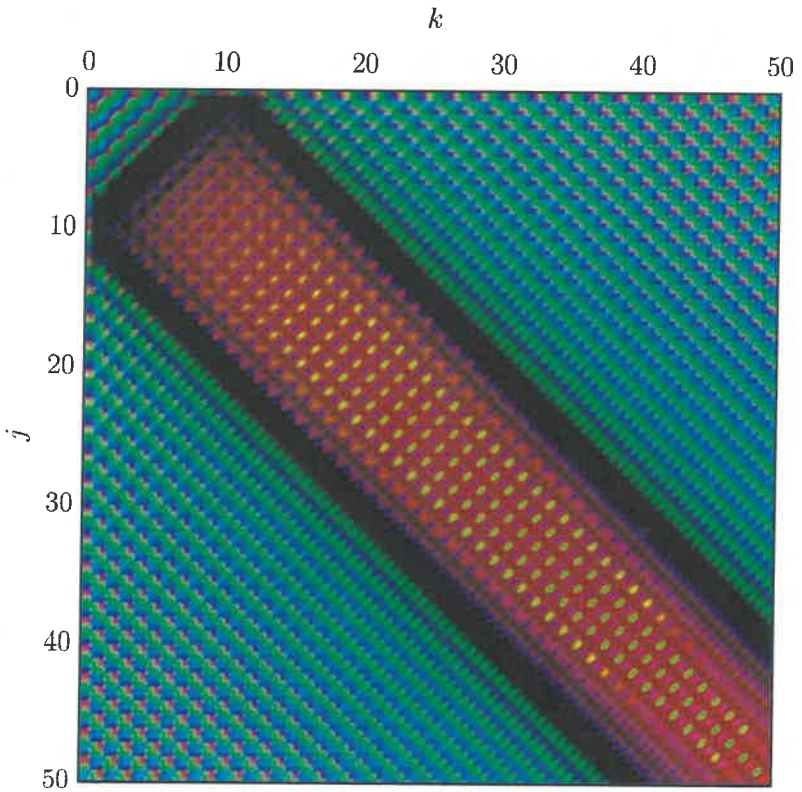

Figure 2. [Colour online] The first 50×50 symmetric submatrix of the energy representation, C_{jk}, of the quench projection operator, $\hat{C} = \mathsf{C}_{jk} |\psi_j\rangle \langle\phi_k|$ which implements the shunt. Illustrated here as a continuous function of j, k, with colour indicating the phase and darkness the magnitude. This is a $q = 10$ quench: note the power is concentrated along the lines satisfying $q^2 = (k \pm j)^2$ - although the function has no poles in j, k space - so that the matrix is banded. The 'reflected' line at the top left corner is understood to be responsible for the mechanism by which a Fermi-gas may be shocked; it arises due to the symmetry of choosing the sinusoidal (rather than exponential) basis, for which the n are natural numbers.

over the zero-temperature Fermi-Dirac distribution. This useful linearity will not of course hold for an interacting gas. In this subsection, we present an overview of the method by which the quenched wavefunction, which we write $\phi_n \to \Phi_n^q$, can be found.

The culmination of this discussion will be an approximation for Φ_n^q given by (9), (10) and (11), from which a consideration of the physics may begin.

A schematic understanding of figure 2 is enough to guess at many of the phenomena that arise during this task: this is because the energy representation in which figure 2 lives can be thought of as the result of folding Fourier-space down the origin, and it is in Fourier (or 'momentum') space that the relevant calculation is most intuitively done. Working, from this point on, in the shunted frame by sending $x \to x - vt$, the quenched state is,

$$\Phi_n^q = \sum_{j=1}^{\infty} \sqrt{\frac{2}{l_0}} \mathsf{C}_{jn} \exp\left(i \left(\frac{1}{2} m v^2 - \frac{\pi^2 j^2}{2 m l_0^2} \right) t + i m v x \right) \sin\left(\frac{j\pi}{l_0} x \right), \quad (4)$$

or, ignoring overall phase factors,

$$\Phi_n^q \propto \sum_{j=1}^{\infty} \frac{\mathsf{C}_{jn}}{i\sqrt{2 l_0}} \exp\left(-i \frac{\pi^2 j^2 t}{2 m l_0^2} \right) \left(e^{\frac{ij\pi}{l_0} x} - e^{-\frac{ij\pi}{l_0} x} \right). \quad (5)$$

The next step is to assume without loss of generality that q is an integer†, removing the need for repetitive translations and caveats. The momentum space is defined by $k = j\pi/l_0$. Using the fact that the continuous version of C_{jn} is odd in j‡, the wavefunction can be written as a sum of four particular contributions: $\tilde{\Phi}_n^q = \tilde{\Phi}_n^{q\,(1)} + \tilde{\Phi}_n^{q\,(2)} + \tilde{\Phi}_n^{q\,(3)} + \tilde{\Phi}_n^{q\,(4)}$. These are shown in Table 1, where $\mathrm{III}_{\frac{\pi}{l_0}}(k)$ is the Dirac comb, $\sum_{j\in\mathbb{Z}} \delta\left(k - \frac{j\pi}{l_0}\right)$, and we define a new envelope function:

$$\tilde{\chi}_n(k) = \frac{\pi}{\sqrt{2 l_0^3} i k} \Big[1 - e^{-i\pi q} \cos(\pi q + l_0 k) - i \left(1 + \frac{l_0 k}{\pi q} \right) e^{-i\pi q} \sin(\pi q + l_0 k) \Big]. \quad (6)$$

Having separated these four terms, we transform back to give the contents of Table 2, in which we have introduced important new physical quantities: the velocities $v_\pm = \pi(n \pm q)/(m l_0)$, wavenumbers $k_\pm = \pi(n \pm q)/l_0$ and frequencies $\omega_\pm = \pi^2 (n \pm q)^2 / 2 m l_0^2$.

†With respect to the results that follow, for the non-interacting case, most quantities of interest (e.g. number density of a degenerate Fermi-gas) can indeed be described by functions which accommodate non-integer particle number, but we won't discuss the generalization here. The case of non-integer q can be solved by slightly re-defining the Dirac combs in Table 1.

‡Therefore, we need not count from $j = 0$ upwards and can use the more comfortable extension over negative wavenumbers.

Table 1. Separating the four contributions to $\tilde{\Phi}_n^q$.

$\tilde{\Phi}_n^{q\ (1)}$	$-\left[\tilde{\chi}_n(k)\,\mathrm{III}_{\frac{\pi}{l_0}}(k)\exp\left(-i\frac{\pi^2(n+q+l_0k/\pi)^2t}{2ml_0^2}\right)\right]*\delta\left(k-\frac{\pi(n+q)}{l_0}\right)$
$\tilde{\Phi}_n^{q\ (2)}$	$\left[\tilde{\chi}_n(-k)\,\mathrm{III}_{\frac{\pi}{l_0}}(k)\exp\left(-i\frac{\pi^2(n+q-l_0k/\pi)^2t}{2ml_0^2}\right)\right]*\delta\left(k+\frac{\pi(n+q)}{l_0}\right)$
$\tilde{\Phi}_n^{q\ (3)}$	$-\left[\tilde{\chi}_n(-k)\,\mathrm{III}_{\frac{\pi}{l_0}}(k)\exp\left(-i\frac{\pi^2(n-q+l_0k/\pi)^2t}{2ml_0^2}\right)\right]*\delta\left(k-\frac{\pi(n-q)}{l_0}\right)$
$\tilde{\Phi}_n^{q\ (4)}$	$\left[\tilde{\chi}_n(k)\,\mathrm{III}_{\frac{\pi}{l_0}}(k)\exp\left(-i\frac{\pi^2(n-q-l_0k/\pi)^2t}{2ml_0^2}\right)\right]*\delta\left(k+\frac{\pi(n-q)}{l_0}\right)$

Table 2. Separating the four contributions to Φ_n^q.

$\Phi_n^{q\ (1)}$	$-l_0\sqrt{\frac{m}{2\pi^3it}}\left[\chi_n(x)*\mathrm{III}_{2l_0}(x)*\delta(x-v_+t)*e^{i\frac{mx^2}{2t}}\right]e^{ik_+x-i\omega_+t}$
$\Phi_n^{q\ (2)}$	$l_0\sqrt{\frac{m}{2\pi^3it}}\left[\chi_n(-x)*\mathrm{III}_{2l_0}(x)*\delta(x+v_+t)*e^{i\frac{mx^2}{2t}}\right]e^{-ik_+x-i\omega_+t}$
$\Phi_n^{q\ (3)}$	$-l_0\sqrt{\frac{m}{2\pi^3it}}\left[\chi_n(-x)*\mathrm{III}_{2l_0}(x)*\delta(x-v_-t)*e^{i\frac{mx^2}{2t}}\right]e^{ik_-x-i\omega_-t}$
$\Phi_n^{q\ (4)}$	$l_0\sqrt{\frac{m}{2\pi^3it}}\left[\chi_n(x)*\mathrm{III}_{2l_0}(x)*\delta(x+v_-t)*e^{i\frac{mx^2}{2t}}\right]e^{-ik_-x-i\omega_-t}$

Taking the inverse Fourier transform we find,

$$\begin{aligned}\chi_n(x) &= \frac{\pi}{2\sqrt{2l_0^3}}\left[\mathrm{sgn}(x)-\mathrm{sgn}(x+l_0)\right]\\ &\quad-\frac{1}{2\sqrt{2l_0}\pi iq}\left[\delta(x+l_0)-e^{-2i\pi q}\delta(x-l_0)\right],\end{aligned}\tag{7}$$

and making use of the associativity and commutativity of the convolution,

$$\begin{aligned}\chi_n(x)*\exp\left(i\frac{mx^2}{2t}\right) &= \frac{1}{2}\sqrt{\frac{\pi^3it}{ml_0^3}}\left[\mathrm{erf}\left(\sqrt{\frac{i^3m}{2t}}x\right)-\mathrm{erf}\left(\sqrt{\frac{i^3m}{2t}}(x+l_0)\right)\right]\\ &\quad-\frac{1}{2\sqrt{2l_0}\pi iq}\left(e^{\frac{im}{2t}(x+l_0)^2}-e^{-2i\pi q+\frac{im}{2t}(x-l_0)^2}\right).\end{aligned}\tag{8}$$

We are therefore left, in the real one-dimensional space of the well, with a sum of four unique plane waves. Each wave is modulated by copies of (8) recurring at intervals of $2l_0$, which are shuttled backwards and forwards over time.

2.3. Interpreting the quenched single particle state

The priority is now to simplify this modulation of the four plane waves. Fortunately, the second term in (8) does not contribute significantly to the behaviour of the state: in the calculation of physical quantities it gives rise to rapidly oscillating terms which may be neglected§. The first term can be thought of as a window function built from complex error functions which decompose into Fresnel integrals. The rapid phase oscillations of these functions greatly complicates the simple qualitative picture¶, and it is possible to work with the real error function as a surrogate. The corners of this window function are softened by the breadth of the error function, of order $\sqrt{t/m}$. The new envelopes are shown in action in figure 3 and figure 4. These very significant simplifications of the results of Section 2.2 leave us with a working model of the shunted wavefunction:

$$\Phi_n^q = \Phi_n^{q\ (1)} + \Phi_n^{q\ (2)} + \Phi_n^{q\ (3)} + \Phi_n^{q\ (4)}, \tag{9}$$

where,

$$\begin{aligned}
\Phi_n^{q\ (1)} &= -\frac{1}{\sqrt{2l_0}}\mathfrak{E}\left(x - v_+t\right)e^{ik_+x - i\omega_+t}, \quad \Phi_n^{q\ (2)} = \frac{1}{\sqrt{2l_0}}\mathfrak{E}\left(-x - v_+t\right)e^{-ik_+x - i\omega_+t}, \\
\Phi_n^{q\ (3)} &= -\frac{1}{\sqrt{2l_0}}\mathfrak{E}\left(-x + v_-t\right)e^{ik_-x - i\omega_-t}, \quad \Phi_n^{q\ (4)} = \frac{1}{\sqrt{2l_0}}\mathfrak{E}\left(x + v_-t\right)e^{-ik_-x - i\omega_-t},
\end{aligned} \tag{10}$$

and the approximate choice of envelope,

$$\mathfrak{E}(x) = \frac{1}{2}\left[\mathrm{erf}\left(\sqrt{\frac{m}{2t}}x\right) - \mathrm{erf}\left(\sqrt{\frac{m}{2t}}(x + l_0)\right)\right] * \mathrm{III}_{2l_0}. \tag{11}$$

In practice (9), (10) and (11) prove to be a very reliable pedagogical model for the quenched state: the qualitative behaviour described below perfectly replicates that observed numerically‖ in states derived purely with the matrix C over a very wide range of parameters.

The principal physical derived quantity of the wavefunction is the number density, $|\Phi_n^q|^2$. To this end, we identify the *compressed phase*, $\Phi_n^{q\ (C)} = \Phi_n^{q\ (1)} + \Phi_n^{q\ (2)}$, and

§It is also suppressed by an $\mathcal{O}\left(1/q\sqrt{t}\right)$ factor with respect to the first term, which may be sufficient cause to discard it with a careful choice of parameters.

¶Furthermore they are notoriously difficult to implement computationally.

‖In Section 3 we will apply the many-body simulation to the non-interacting case, but the time-independent Hamiltonian is easy to implement anyway.

rarefied phase, $\Phi_n^{q\ (R)} = \Phi_n^{q\ (3)} + \Phi_n^{q\ (4)}$, so that $\Phi_n^q = \Phi_n^{q\ (C)} + \Phi_n^{q\ (R)}$. In the evaluation of $|\Phi_n^{q\ (C)}|^2$, the plane waves interfere where the envelopes overlap to give stationary number densities of the form $\sin^2(k_+x)$, which is the expected number density of a particle in the $n+q$ excited state in the shunted frame. Analogously $|\Phi_n^{q\ (R)}|^2$ produces stationary patches of number density proportional to $\sin^2(k_-x)$, the number density of the $n-q$ excited state in the shunted frame. Where and when these 'phases' are manifest in the well is determined by the motion of the envelopes, and consideration of the dependence of the envelope velocities, $v_\pm$, on q leads to the following conclusions:

(i) In the *subsonic* regime, $q \ll n$, the compressed phase develops from the pushed end of the well and the rarefied phase from the pulled end. They encroach on the originally prepared *pristine phase*, (which is of course not stationary in the shunted frame), by compression and rarefaction waves. These waves travel at the overall velocity $n\pi/ml_0$, but their widths grow as $2q\pi t/ml_0$. This regime is shown in figure 3.

(ii) In the *hypersonic* regime, $q \gg n$, both phases develop from the pushed end of the well leaving a natural vacuum at the pulled end. The compressed phase is now a local superposition of two states and is no longer stationary. The compression and rarefaction waves now have velocities $q\pi/ml_0$ and widths $2n\pi t/ml_0$. We may refer to the compressed and rarefied phases and fronts as *shocked* and *antishocked* phases and fronts. This regime is shown in figure 4.

The motivation for the terms 'subsonic', 'hypersonic' and 'shock' is more relevant to the Fermi-gas discussed in Section 2.4. In the non-interacting Fermi-gas, which is collisionless, sound waves propagate as a deformation of the Fermi-surface (or Fermi-points in one dimension), at v_F. In the language of quasi-particles this is considered *zero-sound*. Note that the speed of subsonic fronts in the shunted frame, $n\pi/ml_0$, can be identified as that of the particle in the state ψ_n in the laboratory frame. It is easy to verify that the remaining cross-terms,

$$2\Re\left(\Phi_n^{q\ (1)*}\Phi_n^{q\ (3)} + \Phi_n^{q\ (1)*}\Phi_n^{q\ (4)} + \Phi_n^{q\ (2)*}\Phi_n^{q\ (3)} + \Phi_n^{q\ (2)*}\Phi_n^{q\ (4)}\right), \qquad (12)$$

do indeed account for the number density of the original eigenstate, ψ_n. On top of these phenomena, the edges of the envelopes will be softening over time as described above. Averaging over the density oscillations, it is apparent that in the subsonic case, only the compression and rarefaction fronts have altered average densities, by factors of 3/2 and 1/2 respectively. Of course in the hypersonic case, the regions at

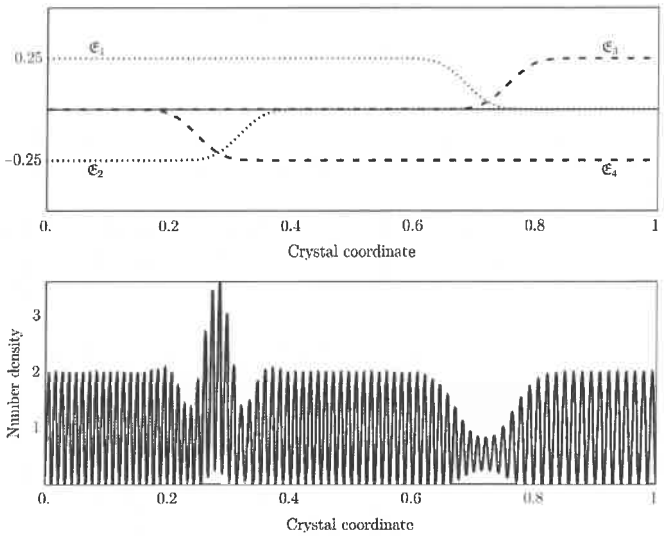

Figure 3. In the shunted frame, the $n = 80$ excited state, ψ_{80}, of the square well shortly after the subsonic left-to-right shunt $q = 10$ to the state Φ^{10}_{80}. [Bottom] The number density, $|\Phi^{10}_{80}|^2$, shows the wavefunction to be partitioned into the compressed, pristine and rarefied phases, separated by compression and rarefaction fronts of altered average number density. [Top] The envelope functions described in (10) and (11) correspond to the features in the wavefunction below.

the pushed and pulled end of the crystal have number density multiplied by 2 and 0. Intermediate regimes such as $q \approx n$ are less satisfying, but by applying the relations in (10) they can be efficiently described.

Returning to our starting point in figure 2, we can now relate the matrix elements to the characteristics of the shunted state. In particular, the upper and lower bands respectively construct the subsonic rarefied and compressed phases. The third 'reflected' band can be thought of as a hypersonic extension of the rarification band and, together with the compression band constructs the shocked phase.

It is desirable to consider other derived quantities which can be written as densities within the well, but here we encounter the very serious limitations of Schrödinger wave mechanics. For example, we have little notion of the temperature of the state, still less of the temperature at different points within it. This is because the system is closed in the shunted frame, rather than coupled to some reservoir, and as it

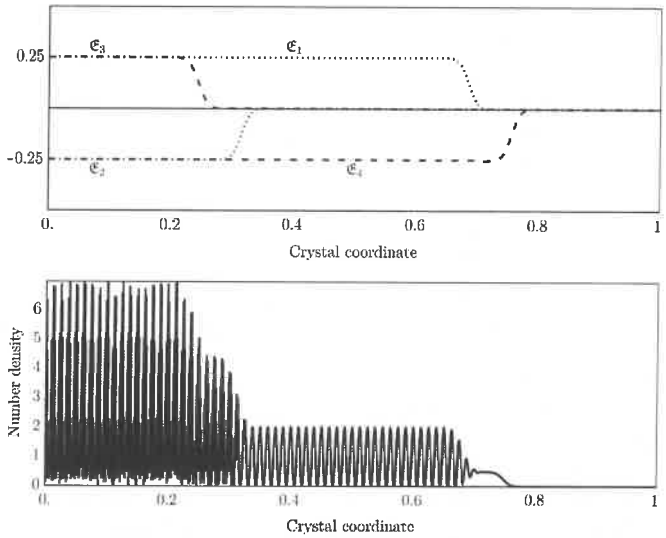

Figure 4. In the shunted frame, the $n = 80$ excited state, ψ_{80}, of the square well shortly after the hypersonic left-to-right shunt $q = 640$ to the state Φ_{80}^{640}. [Bottom] The number density, $|\Phi_{80}^{640}|^2$, shows the wavefunction to be partitioned into the compressed, pristine and rarefied phases, separated by compression and rarefaction fronts of altered average number density. In this hypersonic case, these can be considered shock and anti-shock fronts, the compressed (shocked) phase no-longer resembles a stationary state and the rarefied (anti-shocked) phase is a vacuum. [Top] The envelope functions described in (10) and (11) correspond to the features in the wavefunction below.

exists in a pure rather than mixed state it is not meaningful to form the density matrix. There is however a long tradition of studying the statistical properties of pure states, in particular recent theoretical advances have been made in describing the approach to thermalization, even of energy eigenstates[9]. A cursory glance at figure 3 or figure 4 tells us that the shunted state is far from equilibrium, indeed the compression and rarefaction fronts will travel through each other many times before the system develops a 'temperature'**, far beyond the initial stages of the evolution so far described. Theoretical prescriptions for defining the temperature distribution

**In the long-time picture there arises another problem that has yet to be resolved: is the $1/\sqrt{t}$ behaviour in the envelopes at odds with a finite quantum revival time[12] of the state?

of many-body systems far from equilibrium have been suggested but are still in their infancy[10], [11].

Alternatively we would like to know the stress energy densities associated with the above features and for this we will need a Lagrangian field theory. A less-than satisfying discussion of energy and momentum is confined to Appendix A.

2.4. Assembling the multi-particle picture

The single-particle results of 2.3 can now be applied to construct the multi-particle case. Instead of shunting the nth excited state we will be shunting the non-magnetic, fully degenerate ground state of the Fermi-gas. Neglecting the double-counting from spin considerations, the gas contains N particles, and has a Fermi-wavevector $k_F = N\pi/l_0$ and velocity $v_F = N\pi/ml_0$. We will refer to the regimes $N \gg q$ and $N \ll q$ as being subsonic and hypersonic with respect to the *gas*. It was found in Section 2.3 that the single particle compression and rarefaction fronts have the same velocity in the shunted frame as that associated with the particle in its initial eigenstate. It might therefore be expected that the effects of the shunt on the Fermi-gas will distributed across the spectrum of such velocities present in the gas - as successive fronts extending between the ends of the well and the front associated with the Fermi-velocity. With respect to number density this is found not to be the case.

Formally, the multi-particle state exists in a Slater determinant, but since the time evolution is unitary throughout the shunting process, the shunted states remain orthogonal and the number density of the gas is simply the sum of the number densities of its constituent particles. This will be true even under the influence of interactions. When $N \gg 1$ most of the number density at any point in the well can be accounted for by initial states for which $n \gg 1$, therefore the main consideration will be of average number densities within these states. Take for example the subsonically shunted gas density near the pushed end of the well. In Section 2.3 it was established that the average number density of the subsonically shunted single-particle state is altered only within the compression and rarefaction fronts. It is necessary therefore to sum these corrections to the nth densities over the N states. Since the nth compression wave travels at v_+, which is proportional to n, at any time the total density correction to the gas is given by convolving the average overdensity of a single compression wave

between the pushed end of the well and the Fermi-wavefront, $v_F t$,

$$\Delta\rho(x) = \int_0^N \left[\frac{1}{16}\left(\mathrm{erf}\left(\sqrt{\frac{m}{2t}}(x + \frac{\pi(n+q)}{l_0}t)\right) + 1\right)^2 + \frac{1}{16}\left(\mathrm{erf}\left(\sqrt{\frac{m}{2t}}(-x + \frac{\pi(n+q)}{l_0}t)\right) + 1\right)^2 - \frac{1}{4}\right] \mathrm{d}n. \quad (13)$$

Any shunt subsonic with respect to the gas as a whole is hypersonic with respect to its lowest energy components, however, carefully following the average densities in a single-particle shocked state, we see that (13) is in fact still valid. Similar considerations lead to the following conclusions, which are shown in figure 5:

(i) In the *subsonic* regime, $q \ll N$, the compressed and rarefied gas phases are marked by uniform changes of number density of $\pm q/l_0$. If the envelope softening can be neglected, the gas compression and rarefaction waves are marked by constant density changes which connect the phases, at sharp 'kinks' in the density $\rho(x)$. The compression and rarefaction fronts move at $N\pi/ml_0$, the Fermi-velocity, and their widths grow as $2q\pi t/ml_0$.

(ii) In the *hypersonic* (shocked) regime, the compressed (shocked) gas phase has a maximum number density of $2N/l_0$ and a vacuum forms at the pulled end of the crystal. The fronts move at $q\pi/ml_0$ and have widths $2N\pi t/ml_0$.

We found in 2.3 that the new compressed and rarefied phases of the single-particle state were (locally) physically indistinguishable from stationary states in the shunted frame. So far we have only dealt with average densities of the Fermi-gas, but a similar result will follow if we take into account the density oscillations of the single particle states when we perform the above summation. In Section 2 we introduced the phenomenon of Friedel oscillations in the number density of the Fermi-gas. It can be shown that on the approach to the ends of the potential well, the shunted gas reproduces even these oscillations, corresponding respectively to the $N+q$ and $N-q$ Fermi-gas. This is shown in figure 6.

That the front velocity is equal to the Fermi-velocity is another example of a very general property of the Fermi-gas: the behaviour of the gas is characterised by (that is not to say 'dominated by') the behaviour of its highest occupied state. This is an emergent, collective phenomenon, and occurs without the need for interactions. A basic manifestation of this principle are the Friedel oscillations themselves, whose characteristic wavenumber is the Fermi-wavenumber.

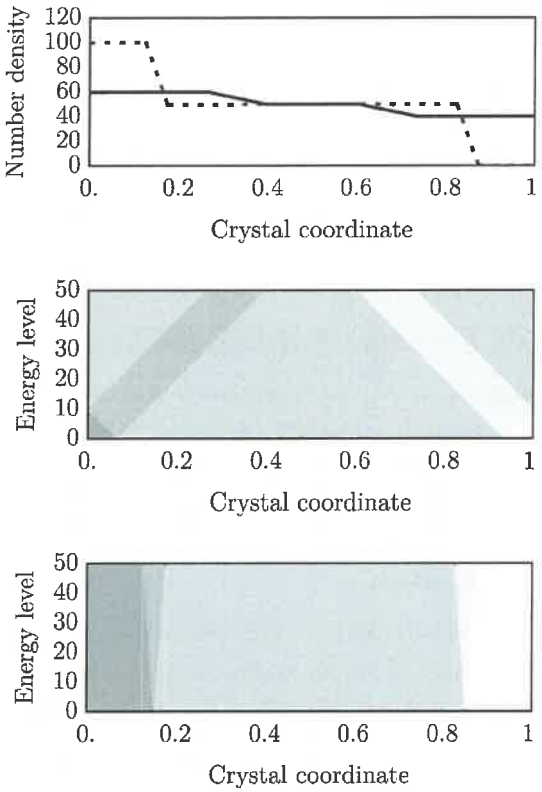

Figure 5. Schematic diagram of shunts acting on the Fermi-gas. [Top] The solid line gives the number density of the subsonic $q = 10$ shunt on the $N = 50$ gas, showing the compressed and rarefied phases of density $(N + q)/l_0$ and $(N - q)/l_0$. The compression and rarefaction fronts are marked by uniform changes of density. The dashed line gives the number density for the hypersonic $q = 300$ shunt on the same gas. The shocked phase has density $2N/l_0$ and a vacuum forms at the far end of the well. [Centre] In the subsonic shunt, each initial energy eigenstate through to N contributes to the density, the shunted states have regions where the initial density is multiplied by 2, 3/2, 1, 1/2 and 0 - shown in grayscale where white represents the vacuum. The gas density is given by summing across these states. [Bottom] The same process for the hypersonic shunt. Notice how, since the shunt is hypersonic with respect to *all* the initial states, a vacuum forms at each energy level.

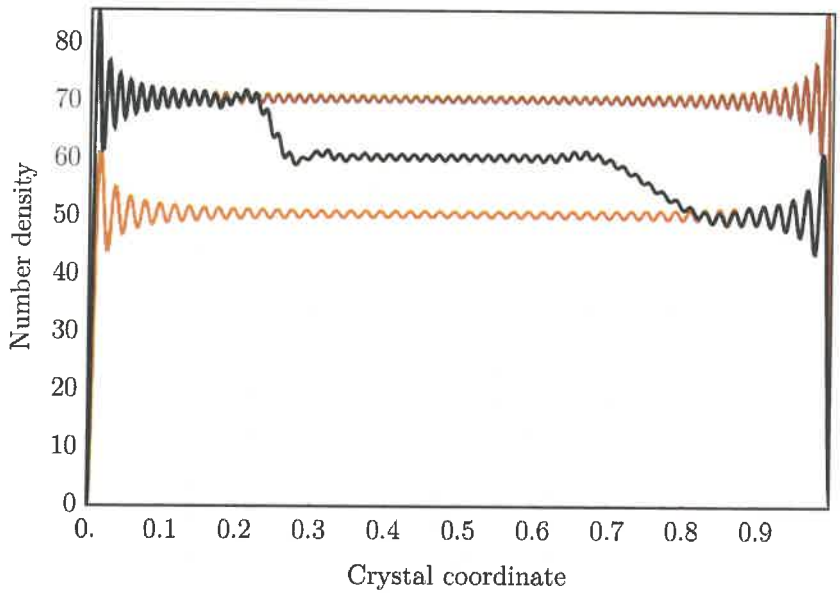

Figure 6. [Colour online] In the shunted frame, number density of the $N = 60$ Fermi-gas having undergone a subsonic $q = 10$ shunt. The compressed and rarefied gas phases agree with the Friedel oscillations of the $N \pm q$ gas ground states. [Black] Number density of the shunted $N = 60$ gas. [Dark orange] Number density of the ground state $N = 70$ gas. [Orange] Number density of the ground state $N = 50$ gas.

To more closely relate the picture of the N-gas in the infinite square well, l_0, to systems found in nature, we can increase both N and l_0 together whilst holding N/l_0 constant; this is the macroscopic limit. The resulting Friedel oscillations will exist at lengthscales far below that of the well itself whilst the overall number density will be unchanged. Note that once interactions are introduced, a natural lengthscale will be set by the Bohr radius. We did not yet consider the relative importance of envelope softening relative to compression, rarefaction, shock and antishock fronts, nor the relative degrees to which these are 'quantum' phenomena. In the present quantum system, this last question may not be a good one: the cold Fermi-gas does not obey the correspondence principle because it is *fundamentally* quantum mechanical††. Re-inserting $\hbar$, the envelopes soften with width $\sqrt{\hbar t/m}$ while subsonic fronts have a width $q\hbar t/ml_0$, so we see that as $\hbar \to 0$ the 'kinked' fronts illustrated in figure 5 should be

††E.g. what is the classical limit of a BEC?

dominated by Fresnel oscillations. The condition for kinked fronts is $q/l_0\sqrt{\hbar t/m} \gg 1$, or if the front is observed when it has traversed a fraction ϵ of the well, $\sqrt{\epsilon}q/\sqrt{N} \gg 1$ and this must be combined with the condition $N \gg q$ to give the correct regime. For the hypersonic case as ever, the roles of q and N are reversed.

3. A Hartree-Fock dispersion relation for the harmonically confined quasi-1D gas

The effect of shunts on the one-dimensional non-interacting Fermi-gas has yielded to a mathematical approach which required very little physical insight: this is partly because it does not represent a realistic physical system. We now try to develop a more reasonable model for an interacting Fermi-gas in which the notion of one-dimensionality can be quantified. Whilst this section forms the basis of the numerical work in Section 3, it does not consider directly the problem of shunts, and it is hoped that it may have more general applications.

3.1. The effective potential of harmonic confinement

We will be concerned with many-body electrostatic interactions. In electrostatics, reduced dimensionality introduces its own problems: the Coulomb potential in two dimensions is logarithmic and in one dimension it is linear. In practice, a one-dimensional quantum system is one in which the dynamics of higher dimensions may be neglected, this is the *quasi-one-dimensional* regime, and in it the Coulomb potential is replaced by an implementation-dependent *effective potential*, $V^{eff}(x)$. A quasi-one-dimensional quantum gas can be constructed from its three dimensional counterpart by enforcing a transverse potential with a spectrum such that, at the temperatures of interest, the occupancies of excited transverse states can be neglected. A very general class of potentials is of course the two-dimensional harmonic oscillator (for the most generic cigar traps), although another highly motivated choice would be the infinite cylindrical well (representing a 'quantum wire'). We will consider the radial harmonic potential of frequency ω. So long as the electrons are known to be confined to the transverse ground state, the single particle wavefunctions are separable in radius, r, and the free axis, x, with charge density obeying $\int \mathrm{d}x\rho_e = (em\omega/\pi)\exp(-m\omega r^2)$. In a gas cooled to degeneracy, two considerations must be made when suppressing the transverse dynamics. The first is the chemical potential. Dividing the gas into

longitudinal and transverse subsystems in thermodynamic equilibrium with each other, we require that the rate of change of occupancy at arbitrarily low temperatures with respect to the energy of the subsystem to be much greater for the gas along the free axis than in the harmonic well:

$$\frac{\mathrm{d}N_l}{\mathrm{d}\mathcal{E}_l} = \frac{2m}{\pi k_F}, \quad \frac{\mathrm{d}N_t}{\mathrm{d}\mathcal{E}_t} = \frac{1}{2\omega}, \quad \frac{4m\omega}{\pi k_F} \gg 1. \tag{14}$$

Secondly the ground state of the harmonic well can be chosen to be much higher than the axial Fermi-energy. This condition will be written for later convenience as

$$\xi^2 \ll 1, \qquad \xi = \frac{k_F}{\sqrt{2m\omega}}, \tag{15}$$

for the (dimensionless) *quasi-one-dimensionality* parameter, ξ. The condition (14) is the real condition for quasi-one-dimensionality, whereas (15) is required for our very simple choice of the radial ground state‡‡. Since $k_F = \pi N/l_0$, a convenient choice of natural units in which $ml_0 = \pi$, used for the numerical work in Section 3, will mean that (15) implies (14), since in a gas N must be numerically large. A discussion of the *shell effects* that result from breakdown of quasi-one-dimensionality is given in [2]. The effective pair potential along the axis is equivalent to the energy stored in a parallel-plate capacitor with axisymmetric Gaussian charge density:

$$V^{eff}(x) = e^2 \left(\frac{m\omega}{\pi}\right)^2 \int \mathrm{d}^2x_1 \int \mathrm{d}^2x_2 \frac{\exp\left[-m\omega\left(|\mathbf{x}_1|^2 + |\mathbf{x}_2|^2\right)\right]}{\sqrt{x^2 + |\mathbf{x}_1 - \mathbf{x}_2|^2}}. \tag{16}$$

Since this is evaluated over infinite limits, a simple translation of the variables gives

$$\begin{aligned} V^{eff}(x) &= e^2 \left(\frac{m\omega}{\pi}\right)^2 \int \mathrm{d}^2x_1 \int \mathrm{d}^2x_2 \frac{\exp\left[-m\omega\left(2|\mathbf{x}_1|^2 + |\mathbf{x}_2|^2/2\right)\right]}{\sqrt{x^2 + |\mathbf{x}_2|^2}} \\ &= e^2 m\omega \int_0^\infty \mathrm{d}r \frac{r \exp\left(-m\omega r^2/2\right)}{\sqrt{x^2 + r^2}} \\ &= \sqrt{\pi} e^2 \eta \exp\left(\eta^2 x^2\right) \operatorname{erfc}\left(\eta|x|\right), \end{aligned} \tag{17}$$

where $\operatorname{erfc}(x)$ is the complimentary error function and $\eta = \sqrt{m\omega/2}$, the *confinement parameter*, is a characteristic wave number of the harmonic well - indeed $1/2\eta = \sigma$ for the radial variance of the density, σ^2; a modern nanowire might have $\eta \approx 10^5$ cm^{-1}, but this is far too low. Most metals have a Fermi-wavevector of order $k_F \approx 10^8$ cm^{-1},

‡‡More accurately, ξ should be less than 2 to prevent occupancy of the first excited harmonic state at low temperatures.

for which (15) would require a wire of atomic width, on the level of the Angstrom§§. The two variables ξ and η are related by the Fermi-wavevector, $\xi = k_F/2\eta$.

The new potential (17) is generally well-behaved at the origin and vanishes at infinite separation. Note however that its integral does not converge, while its transformation under η is area-preserving. In the limit $\eta \to \infty$ the system describes point particles on a wire, for which, applying l'Hopital's rule away from the origin, we recover the expected Coulomb potential,

$$x \neq 0, \quad \lim_{\eta\to\infty} V^{eff}(x,\eta) = \frac{\sqrt{\pi}e^2}{|x|} \lim_{y\to\infty} y \exp\left(y^2\right) \operatorname{erfc}\left(|y|\right) = \frac{e^2}{|x|}.$$

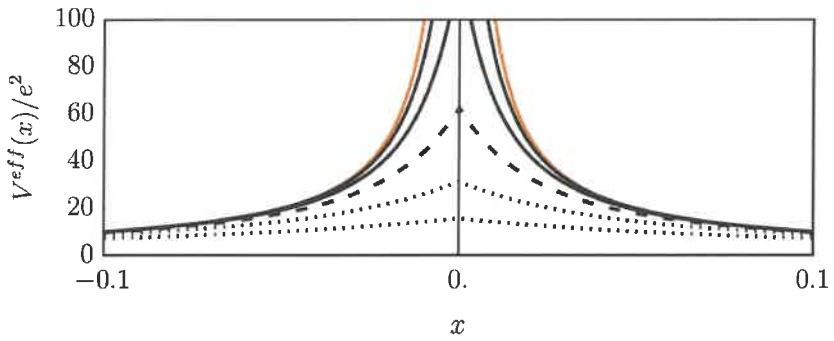

Figure 7. [Colour online] The logarithmic singularity of the Coulomb potential (orange) is removed if the particles are assumed to be in transverse harmonic ground states. From top to bottom $\xi = 0.25, 0.5, 1, 2, 4$.

3.2. The exchange potential

At this point we choose to be dealing with a simple jellum theory: the axial potential is assumed to be uniform, and to cancel with the Hartree potential. In three dimensions the Hartree-Fock eigenstates of Coulomb-jellium are plane waves. Applying this principle to the quasi-one-dimensional case, the spectrum is to be given by

$$\mathcal{E}_k = \frac{k^2}{2m} + V_k^X \tag{18}$$

§§However, the bulk properties of a metal may no longer apply at this scale.

where, with $E_1(x)$ as the exponential integral function, the exchange contribution can be written¶¶

$$V_k^X = -\frac{e^2}{2\sqrt{\pi}}\eta \int_{-\infty}^{\infty} \mathrm{d}x' \int_{-k_F}^{k_F} \mathrm{d}k' \left[e^{-i(k-k')x' + \eta^2 x'^2} \mathrm{erfc}\left(\eta |x'|\right) \right]$$
$$= \frac{e^2}{2\pi} \int_{-k_F}^{k_F} \mathrm{d}k' \exp\left[\frac{(k-k')^2}{4\eta^2}\right] E_1\left[\frac{(k-k')^2}{4\eta^2}\right]. \tag{19}$$

In order to resolve this non-standard integral and write (19) in the final usable form (25), we make use of the Leibniz rule by positing the antiderivative,

$$\mathfrak{G}(x) = \frac{\sqrt{\pi}}{2} \mathrm{erfi}(x) E_1(x^2) + \mathfrak{F}(x), \tag{20}$$

for the odd function $\mathfrak{F}(x)$ such that $\frac{\mathrm{d}}{\mathrm{d}x}\mathfrak{F}(x) = -(\sqrt{\pi}/2)\mathrm{erfi}(x)\frac{\mathrm{d}}{\mathrm{d}x}E_1(x^2)$. To proceed, a series expansion for such an $\mathfrak{F}(x)$ must give,

$$\frac{\mathrm{d}}{\mathrm{d}x}\mathfrak{F}(x) = \sum_{l=0}^{\infty}(2l+1)a_l x^{2l} = 2\sum_{n=0}^{\infty}\frac{x^{2n}}{(2n+1)n!}\sum_{n=0}^{\infty}\frac{(-1)^m x^{2m}}{m!}, \tag{21}$$

and following Frobenius' prescription for solving ODEs, the coefficients a_l are given by equating powers:

$$a_l = \frac{2(-1)^l}{(2l+1)l!}\sum_{n=0}^{\infty}\frac{(-1)^n}{(2n+1)}\binom{l}{n}. \tag{22}$$

Applying a well known combinatorial identity for the reciprocal of a binomial coefficient***,

$$\binom{j+k}{k}^{-1} = \sum_{i=1}^{k}(-1)^{i-1}\frac{i}{j+i}\binom{k}{i}, \tag{23}$$

the series can be written,

$$a_l = \frac{2(-1)^l}{(2l+1)(l+1)l!}\binom{l+\frac{1}{2}}{l+1}^{-1} = \frac{(-2)^{l+2}(l+1)!}{(2l+1)\left[2(l+1)\right]!}, \tag{24}$$

where the last equality employs the Gamma function of half-integer arguments. By considering the ratio of consecutive coefficients, $a_{l+1}/a_l = -(\frac{1}{2}+l)/(\frac{3}{2}+l)^2$,

¶¶Indeed, the integrand of (19) is mentioned in [1] as being the form factor of the transverse number density for just such a wire.

***See, for example, Gould's book: [13].

this series is recognizable as the generalized hypergeometric function, $\mathfrak{F}(x) = 2x_2F_2\left(\frac{1}{2}, 1; \frac{3}{2}, \frac{3}{2}; -x^2\right)$, so that the exchange potential may be written:

$$V_k^X = \frac{e^2\eta}{\pi}\left[\frac{\sqrt{\pi}}{2}\mathrm{erfi}(x)E_1(x^2) - 2x_2F_2\left(\frac{1}{2}, 1; \frac{3}{2}, \frac{3}{2}; -x^2\right)\right]_{\frac{k-k_F}{2\eta}}^{\frac{k+k_F}{2\eta}}. \tag{25}$$

3.3. The dispersion relation

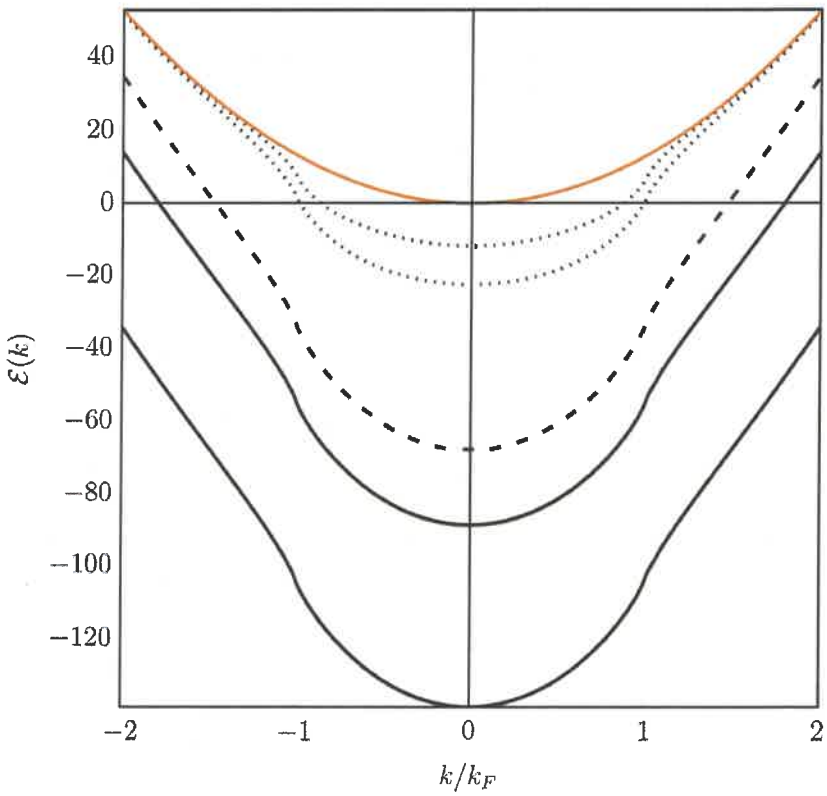

Figure 8. [Colour online] The parabolic dispersion of free particles is in orange. From top to bottom $\xi = 0.1, 0.5, 1, 5, 10$.

The potential (25) is remarkably similar to the well-known dispersion relation of three-dimensional jellium[17]. The renormalized mass of low energy Hartree-Fock

particles in the $|k| \to 0$ limit is given by the curvature,

$$m^* = \lim_{k\to 0} \frac{m}{1 + m\frac{\mathrm{d}^2}{\mathrm{d}k^2} V_k^X}. \tag{26}$$

In the present case the correction is

$$\lim_{k\to 0} m\frac{\mathrm{d}^2}{\mathrm{d}k^2} V_k^X = \frac{2r_s}{a_B}\left[1 + \xi^2 e^{\xi^2} E_1\left(\xi^2\right)\right], \tag{27}$$

where $r_s = \pi/4k_F$ is the separation of Hartree-Fock particles in the very cold, non-magnetic Fermi-gas and $a_B = 1/me^2$ is the Bohr radius. The contribution in ξ must be an artefact of the confinement since it is the only manifestation of η, and apparently vanishes as $\eta \to 0$. Conversely the effective mass of low-energy Hartree-Fock particles is reduced to $m^*/m = 1/(1 + 2r_s/r_B)$ in the strongly confined limit of point particles. The analogous effect in three dimensional Coulomb-jellium is significantly weaker, with $m^*/m \approx 1/(1 + 0.22r_s/r_B)$.

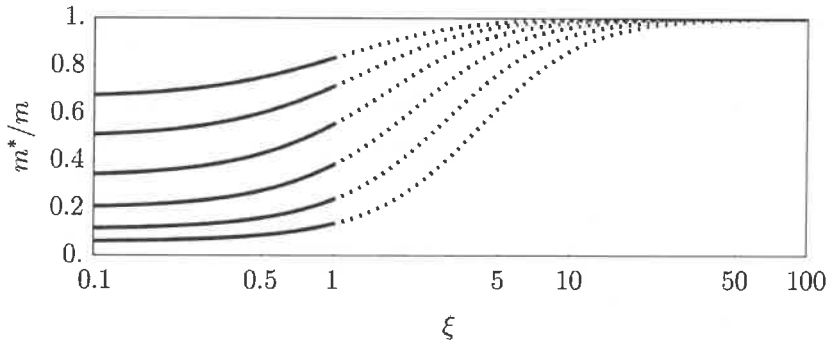

Figure 9. The effective mass of low-energy Hartree-Fock particles is reduced by confinement. From top to bottom $r_s/a_B = 1/2$, 1, 2, 4, 8, 16.

As in three-dimensional jellium, the band width of occupied states is increased by the exchange interaction. The ratio of the interacting bandwidth, $\mathcal{E}_{HF}$ to that of free fermions, $\mathcal{E}_0$ is given by

$$\frac{\mathcal{E}_{HF}}{\mathcal{E}_0} = 1 + \frac{2}{\pi^2}\frac{r_s}{a_B}\frac{1}{\xi}\left[\mathfrak{G}(2\xi) - 2\mathfrak{G}(\xi)\right]. \tag{28}$$

and for $\xi^2 \ll 1$ the band width approaches $\mathcal{E}_{HF}/\mathcal{E}_0 = 1 + (2\ln 2/\pi^2)(r_s/a_B)$, or $\mathcal{E}_{HF}/\mathcal{E}_0 \approx 1 + 0.14(r_s/a_B)$, however the result for three dimensional Coulomb jellium is now stronger, being $\mathcal{E}_{HF}/\mathcal{E}_0 \approx 1 + 1.22(r_s/a_B)$.

In order to relate to the degenerate Fermi-gas discussed in Section 2 we will not be concerned with $r_s/a_B \gg 1$. The above theory could in principle be extended with an expansion for the energy density of the electron gas with respect to r_s/a_B, and a discussion of magnetic phases and quasi-one-dimensional Wigner-crystallization.

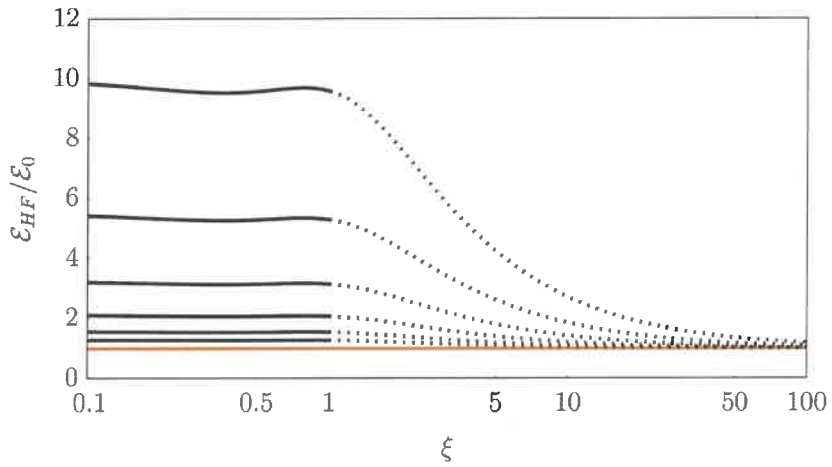

Figure 10. [Colour online] The band-width of the wire relative to that of free particles. From bottom to top $r_s/a_B = 1/2$, 1, 2, 4, 8, 16.

A final important observation is that the group velocity is singular at k_F, since the gradient under the integral sign of (19) is,

$$\frac{\mathrm{d}}{\mathrm{d}k}V_k^X = \frac{e^2}{2\pi}\left[\exp(x^2)E_1(x^2)\right]_{\frac{k-k_F}{2\eta}}^{\frac{k+k_F}{2\eta}}. \tag{29}$$

This clearly absurd effect is also famously predicted for 3D Coulomb-Jellium. It is understood to be caused by the fact that Coulomb interactions are long range. Whilst the $V^{eff}(x)$ of the harmonic wire suppresses the singular origin of the Coulomb potential (this is the feature that enables us to evaluate the Hartree and exchange integrals in Section 4), it does not suppress the asymptotes, and the theory of the exchange potential developed here will be badly incomplete without consideration of electron screening.

4. Interacting Fermi-gas: time-dependent Hartree-Fock theory

4.1. Phenomenology of the quenched state

In this section we present qualitative observations of shunts in the system described in Section 3, where the infinite square well is imposed on the free axis; this can be thought of as taking a quantum wire of finite length. Details of the system and of the numerical methods used are confined to Section 4.2 and Appendix A. These results are interpreted under the concluding remarks in Section 5.

TDHFT was implemented in a basis of $d = 100$ for Fermi-gases of roughly $N = 50$ electrons, interacting under the $V^{eff}(x)$ in (17) with quasi-one-dimensionality $\xi = 1$. Electron charge, q, was taken as a free parameter.

The interacting ground states could be found very effectively by applying convergent Hartree-Fock theory. As the charge is 'switched on', the electron repulsion forces the ground state gas towards the walls of the well, resulting in a 'meniscus'. A key result of the non-interacting theory in Section 2 was that the compressed phase approached the ground state of the $N + q$ gas near the pushed wall, reproducing even the Friedel oscillations, and it was found that this principle extends to the interacting case, shown in figure 11. Remarkably, this behaviour could be observed even when the prepared state was *not* an interacting ground state: the compression wave reliably left behind an ultracold $N + q$-Fermi-gas.

The dependence of the velocity of the compression or shock front, $v^{(C)}$, on the interaction strength was studied for various shunts, with examples shown in figure 12. For subsonic shunts, $v^{(C)}$ was linear in the interaction strength. The relationship was not affected by the shunt speed so long as it was subsonic (within reason: the quality of the data was reduced for fast subsonic shunts), indicating that the dependence is a property of the *gas* itself. For hypersonic shunts no such general relationship could be observed. Qualitatively, the speed of the shock front was often *reduced* by the interactions, and it was *not* a gas property.

For increasing Fermi-velocity in the gas, the relative deviation in $v^{(C)}$ was found to be monotonically decreasing as shown in figure 13.

4.2. Methods for TDHFT in the infinite square well

The implementation of TDHFT generally presents two principal computational challenges: formation of the Fock matrix and unitary time evolution. During the

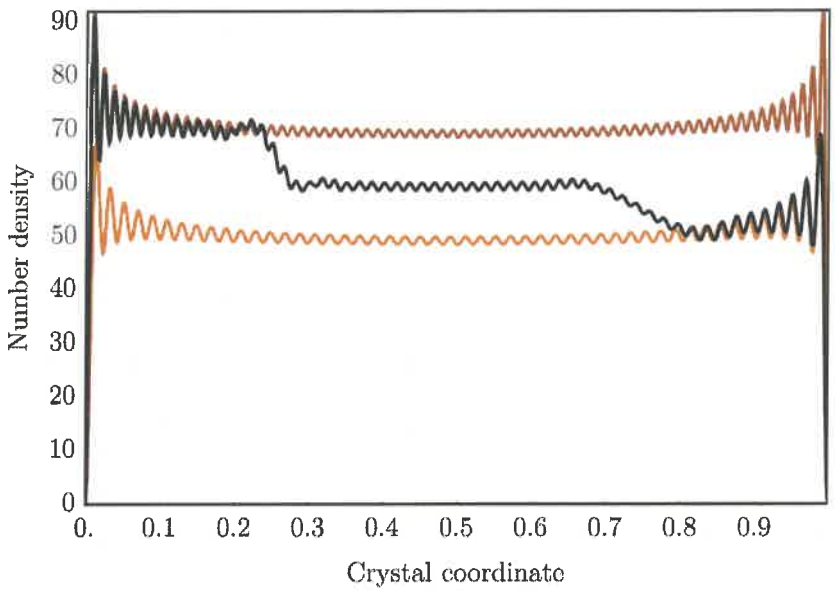

Figure 11. [Colour online] In the shunted frame, number density of the $N = 60$ electron gas in a length of wire having undergone a subsonic $q = 10$ shunt. The compressed and rarefied gas phases agree with the Friedel oscillations and meniscus of the $N \pm q$ gas ground states. [Black] Number density of the shunted $N = 60$ gas. [Dark orange] Number density of the ground state $N = 70$ gas. [Orange] Number density of the ground state $N = 50$ gas.

post-shunt time evolution of the system we work in the 'shunted' frame in which the well is stationary. In this frame we can define the *atomic basis*, $|\psi_n\rangle$, where the ψ_n are as defined in Section 2. This basis corresponds to the non-interacting energy representation, and numerically we must impose an upper cut-off, working with its first d elements. At any time the N-particle Fermi-gas exists as a multi-particle state in the form of a Slater determinant, with single-particle wavefunctions $|\chi_n\rangle$, this we call the *molecular basis*. The terms 'molecular basis' and 'atomic basis' are conventions from quantum chemistry. In the atomic basis the multi-particle state can be represented by the $d \times N$ matrix, $\mathsf{S}_{jk} = \langle\psi_j|\chi_k\rangle$. The Fock matrix is the Hartree-Fock approximation for the Hamiltonian, in the absence of external potentials it takes the form,

$$\mathsf{H}_{jk} = \mathsf{h}_{jk} + \mathsf{U}^{(H)}_{jk} + \mathsf{U}^{(E)}_{jk}, \tag{30}$$

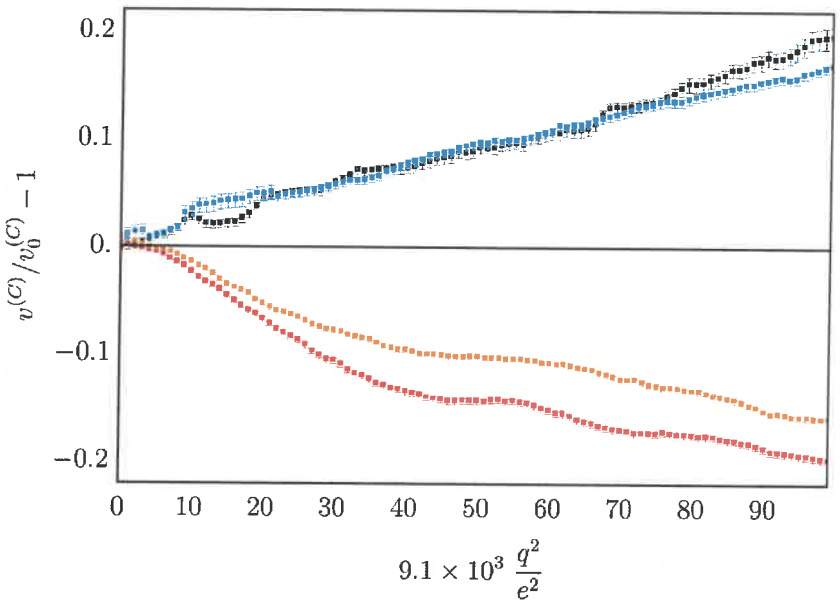

Figure 12. [Colour online] Relative deviation in compression and shock front velocities, $v^{(C)}$, (from non-interacting theory, $v_0^{(C)}$) in the quantum wire as the electron charge, q, is increased, for various choices of Fermi-velocity, v_F, and shunt velocity, v. [Blue] Subsonic shunt: $N = 50$, $q = 10$, $v = 0.2v_F$. [Black] Subsonic shunt: $N = 50$, $q = 20$, $v = 0.4v_F$. [Red] Hypersonic shunt: $N = 30$, $q = 50$, $v = 1.7v_F$. [Orange] Hypersonic shunt: $N = 20$, $q = 60$, $v = 3v_F$. The 'scalloped' variations in the subsonic $v^{(C)}$ are thought to be an artefact of Friedel oscillations moving near the compression front, see Section 4.2.

where h is the usual Laplacian Hamiltonian of free particles and $\mathsf{U}^{(H)}$ and $\mathsf{U}^{(E)}$ are matrices of the *Hartree* and *exchange* operators defined (using the summation convention) by,

$$\mathsf{U}^{(H)}_{jk} = \langle\psi_j|\,\langle\chi_l|\,\hat{G}\,|\chi_l\rangle\,|\psi_k\rangle\,, \quad \mathsf{U}^{(E)}_{jk} = \langle\psi_j|\,\langle\chi_l|\,\hat{G}\,|\psi_k\rangle\,|\chi_l\rangle\,, \tag{31}$$

with the pair interaction given by the operator $\hat{G}$. In real space, $\hat{G}$ appears as the kernel $V^{eff}(x_1 - x_2)$, and in the atomic basis as a fourth rank Cartesian tensor, $\mathsf{G}_{ijkl} = \langle\psi_i|\,\langle\psi_j|\,\hat{G}\,|\psi_k\rangle\,|\psi_l\rangle$. The matrix elements in (31) are known as the *Hartree integrals* and *exchange integrals*, using the outer product, $\mathsf{P} = \mathsf{S}\mathsf{S}^\dagger$, they can be written as variations on the same contraction:

$$\mathsf{U}^{(H)}_{jk} = \mathsf{G}_{jlmk}\mathsf{P}_{lm}, \quad \mathsf{U}^{(E)}_{jk} = \mathsf{G}_{jlkm}\mathsf{P}_{lm}. \tag{32}$$

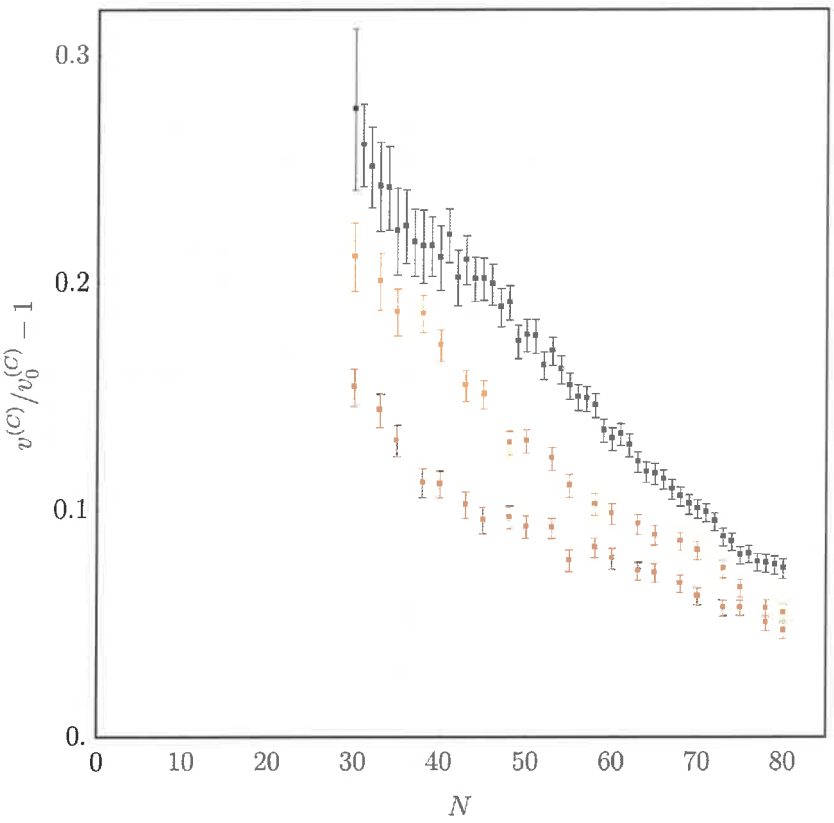

Figure 13. [Colour online] Relative deviation in compression and shock front velocities, $v^{(C)}$, (from non-interacting theory, $v_0^{(C)}$) in the quantum wire against a variable number, N, of electrons, for three choices of electron charge, q. [Black] $q^2/e^2 = 9.9 \times 10^{-3}$. [Orange] $q^2/e^2 = 7.7 \times 10^{-3}$. [Dark orange] $q^2/e^2 = 5.5 \times 10^{-3}$.

We can further define the d^2 matrices $\Lambda_{jk|lm} = \mathsf{G}_{jlmk}$ and $\Pi_{jk|lm} = \mathsf{G}_{jlkm}$ so that,

$$\mathsf{U}_{jk}^{(H)} = \mathrm{Tr}\ \Lambda_{jk}\mathsf{P}, \quad \mathsf{U}_{jk}^{(E)} = \mathrm{Tr}\ \Pi_{jk}\mathsf{P}. \tag{33}$$

This last step is mathematically trivial but computationally useful, because if we have the relevant Λ, Π and P to hand, the evaluation of a Fock matrix element is the same as taking a d-dimensional trace. Many programming languages support optimized routines for matrix algebra, but *not* tensor algebra. In order to assemble a library of the Λ_{jk} and Π_{jk} we must still evaluate all the elements of G; this is an $\mathcal{O}(d^4)$ task, but

is made 2^3 times easier by the symmetries of G. More importantly we may exploit the real space form of the atomic basis:

$$\mathsf{G}_{ijkl} = \frac{4}{l_0^2}\int_0^{l_0}\int_0^{l_0} \mathrm{d}x_1\mathrm{d}x_2[\mathrm{s}_i(x_2)\mathrm{s}_j(x_1)V^{eff}(x_1-x_2)\mathrm{s}_k(x_1)\mathrm{s}_l(x_2)], \quad (34)$$

where $\mathrm{s}_n(x) = \sin(n\pi x/l_0)$. By inspecting the form of (34), it is clear that the G_{ijkl} can be thought of as a sum of sixteen points in k-space of the double Fourier transform,

$$\Gamma(k_1,k_2) = \int\int \mathrm{d}x_1\mathrm{d}x_2\left[V^{eff}(x_1-x_2)w(x_1)w(x_2)e^{-i(k_1x_1+k_2x_2)}\right], \quad (35)$$

where $w(x)$ is the window function extending from 0 to l_0. This is an example of Plancherel's theorem. Since the points to be sampled are of the form $(j\pi/l_0, k\pi/l_0)$ for integer j, k, it should only be necessary to calculate the discrete Fourier transform, equivalent to the periodic extension of $V^{eff}(x_1-x_2)$ over the two-dimensional lattice with parameter $2l_0$. This calculation lends itself well to the Fast Fourier Transform (FFT).

For our applications, it was not usually necessary to perform more than 10^2 time steps in any simulation, allowing us to use the full unitary time-evolution operator, $\mathsf{U} = \exp(-i\mathsf{H}\delta t)$, which enforces the conservation laws of $\hat{H}$. Instead, the bottleneck formed at the point of reading the Λ_{jk}/Π_{jk} libraries at each iteration: a practical balance was struck with a $d = 100$ basis.

In order to measure the position of the compression front, the front itself must be defined. From Section 2 it was understood in the subsonic, non-interacting case, to be the region of transition in number density, $\rho(x,t)$, from that of the compressed gas phase, $\rho^{(C)}(x,t)$, to the pristine gas phase, $\rho^{(P)}(x,t)$. A clearer picture of this transition (which suppresses the Friedel oscillations) is given by the measure, $\tau(x,t) = \left[\rho(x,t)-\rho^{(P)}(x,t)\right] / \left[\rho^{(C)}(x,t)-\rho^{(P)}(x,t)\right]$, so that near the pushed wall and the centre of the well, $\tau(x,t)$ should approach 1 and 0 respectively. The 'front' might then be taken as the normalized first moment of $\partial_x\tau(x,t)$ within the first half of the well:

$$x_f = \frac{\frac{l_0}{2}\tau(l_0/2,t) - \int_0^{l_0/2}\mathrm{d}x\tau(x,t)}{\tau(l_0/2,t)-1}. \quad (36)$$

A study of the non-interacting regime is merely the evaluation of a pre-determined† † † function rather than a simulation, and my be conducted to arbitrarily high precision.

† † †I.e. pre-determined, by the matrix C in Section 2.

The measure in (36) was found to be in excellent agreement with the established non-interacting result that $\dot{x}_f = v_F$, however is was not reliable for hypersonic shunts due to the time-dependent nature of the shocked phase. Instead it was generally necessary to measure the shock front by solving $\rho(x,t) - \rho^{(P)}(x,t) = c$ for $x = x_s$ at various c. A more serious problem was presented by the fact that, at $N = 50$ Fermions, even $\tau(x,t)$ was not usually monotonic near the front. As a result, x_f had a tendancy to follow 'false peaks' in $\tau(x,t)$: the value of $\dot{x}_f$ may change very smoothly with the parameters until a change of peak, at which point there will be a discontinuity. The errors shown in figure 12 are sensitive to this, however (the same effect causes periodic 'braiding' in the $x_f(t)$ measurements which reduces the quality of the linear regression calculated for each point), which gives them an oversized appearance, relative to the (local) smoothness of the plot.

Within natural units, it is very convenient computationally to choose a scale for energy, $\mathcal{E}_0$ in which $m_e = \pi\mathcal{E}_0$ and $l_0 = \mathcal{E}_0^{-1}$. This gives $\mathcal{E}_0 \approx 2.61 \times 10^{-7}$ erg, so that we work in a well of length $l_0 \approx 2.61 \times 10^{-9}$ cm, or a quantum wire of perhaps only 10^2 atoms. This is far smaller than modern nanowires, and in order for the behaviour of the electron gas to be qualitatively relatable to that of the non-interacting Fermi-gas described in Section 2, the electron charge must be reduced by a factor of roughly 10^{-3}. The corresponding increase in the Bohr radius should guarantee that we are in the high density regime of the electron gas, where the behaviour is dominated by the kinetic energy.

5. Concluding remarks

Schrödinger's wave mechanics have provided a remarkably clear picture of the non-interacting shunted gas. A very cold one-dimensional Fermi-gas, when pushed or pulled consistently at a speed below the Fermi-velocity, changes phase to regions of altered number density via wave-fronts that spread *at* the Fermi-velocity in the moving frame. Furthermore these new phases are, to an excellent approximation, ground states of the gas with respect to this number density. Conversely if the gas is shocked, the shockwave moves at the speed of the applied potential in the moving frame (twice the shock speed in the laboratory frame). The shock leaves behind an excited state of twice the initial number density and the anti-shock leaves behind a vacuum.

The physical quasi-one-dimensional electron gas is a far more complicated system.

Considering only the exchange interaction within Hartree-Fock theory it is apparent that the spectrum of the quantum system and all its properties are greatly altered, however since we have not taken shielding into account the picture is far from finalized.

Hartree-Fock theory is well suited to quantum many-body systems confined to the infinite square well: it is possible to quickly calculate the integrals relevant to the formation of the Fock matrix in advance, to arbitrary precision, and to do so for a general pair potential.

TDHFT in an unshielded quantum wire supports the behaviour predicted in the non-interacting Fermi-gas subjected to pushes and pulls below the Fermi-velocity. Of particular interest is the unexplained 'cooling' of the new phases to their respective ground states.

Interactions increase the speed of compression fronts in subsonic shunts, the speed is seen to be linear in the interaction strength (the square of the electron charge). As was mentioned in section 3, the unshielded interaction potential is long range; in one dimension its (single body) scattering length diverges[16]. Consequently, perturbative waves in the number density must be considered collisional at all wavelengths, giving rise to the phenomenon of *first sound*. The form of the relationship observed in figure 12 is that expected for the speed of first sound waves, as mentioned in [2]. Furthermore as the kinetic energy of the gas increases the enhancement of first sound speed should be 'drowned out', which may explain figure 13. This would be a satisfying development of the implicit understanding of zero sound for subsonic and hypersonic shunts in the non-interacting gas. However, since our approach was to simply export the bare Coulomb potential of the quasi-one-dimensional system into a numerical many-body method, we cannot truly qualify the nature of interacting compression fronts. Particularly, we can offer no formal relationship between the dispersion relation (19) and the propagation of the interacting compression fronts without a consideration of screening effects.

If the harmonically confined wire is considered useful, the effects hinted at here may be elucidated by a study of its dielectric response function. Efforts in this direction have already been made, for example in [1]. Such considerations may provide our TDHFT implementation with a better-motivated choice of screened potential, a task which goes beyond the scope of this project.

It is hoped that work may be undertaken in the near future to consider the analogous problem involving Floquet theory (see e.g. [18]), where the well moves relative to stationary ionic potentials.

Acknowledgments

I am grateful to Emilio Artacho and Rao Peng for many useful conversations.

Appendix A. Derived quantities in the Schrödinger picture

Unfortunately there is no unique Lagrangian density for the Schrödinger equation[15], [14], but a common choice is,

$$\mathcal{L} = \frac{i}{2}\left(\psi^*\dot{\psi} - \psi\dot{\psi}^*\right) - \frac{1}{2m}\partial_x\psi^*\partial_x\psi, \tag{A.1}$$

for a generic wavefunction ψ, so that the Hamiltonian density is $\mathcal{H} = \partial_x\psi^*\partial_x\psi/2m$‡‡‡ and the momentum density $\mathcal{P} = -i\psi^*\partial_x\psi$. By way only of example, we confine our attention to the subsonic compression front at times when the envelopes are 'sharp' with respect to other length scales. The wavevunction could locally be written,

$$\sqrt{2l_0}\Phi_n^q = \mathfrak{E}\left(x - v_+t\right)e^{ik_+x - i\omega_+t} + e^{-ik_+x - i\omega_+t} + \mathfrak{E}\left(-x + v_-t\right)e^{ik_-x - i\omega_-t}. \tag{A.2}$$

By averaging over wave cycles the momentum density is,

$$\begin{aligned}\langle\mathcal{P}\rangle = {} & k_+|\mathfrak{E}\left(x - v_+t\right)|^2 + k_-|\mathfrak{E}\left(-x + v_-t\right)|^2 - k_+ \\ & -i\mathfrak{E}\left(x - v_+t\right)^*\partial_x\mathfrak{E}\left(x - v_+t\right) - i\mathfrak{E}\left(-x + v_-t\right)^*\partial_x\mathfrak{E}\left(-x + v_-t\right).\end{aligned} \tag{A.3}$$

According to the first two terms the compression front absorbs the momentum density of the original phase at a rate $2\pi^2q(n+q)/ml_0^2$ and accumulates its own momentum at a rate $2\pi^2q(n-q)/ml_0^2$. This momentum is stored at a uniform density within the width of the wave. The last two terms of (A.3) describe distributions of momentum at either end of the wave that average to zero. Conservation of momentum can be demonstrated by repeating this process for the rarefaction wave and considering the differential forces applied to either end of the well - which can be inferred by the fact that the compressed and rarefied phases are locally stationary states with differing, well defined pressure. The fact that the applied force is constant as the fronts traverse the well is interesting from the point of view of the projectile that is being modelled.

A similar study of the Hamiltonian density yields the compression wave energy distribution,

$$\langle\mathcal{E}\rangle = \frac{1}{2m}\Big(k_+^2|\mathcal{E}\left(x - v_+t\right)|^2 + k_-^2|\mathcal{E}\left(-x + v_-t\right)|^2 + k_+^2$$

‡‡‡This can be derived by applying parts to the expression for the Hamiltonian expectation from the spatial wavefunction.

$$+|\partial_x \mathcal{E}(x - v_+ t)|^2 + |\partial_x \mathcal{E}(-x + v_- t)|^2\Big). \tag{A.4}$$

This in particular shows that there is a Gaussian-shaped distribution of energy localised at either end of the compression wave, which is associated with the envelope edges. The picture of momentum and energy densities near the boundaries of the compression wave are necessarily imperfect due to the envelope approximations made in (11).

Since this report involves discussion of the shocked Fermi-gas, a simple application of Schrödinger field theory is to verify the Rankine-Hugoniot relations apply throughout the shock width. However the calculations are not necessarily so instructive because the Hamiltonian already implies the conservation laws, and because we already know the characteristics of the phases either side.

Appendix B. TDHFT implementation in C++

The TDHFT implementation used in Section 4 was written in C++14. Extensive use is made of the GNU Scientific Library (GSL), in particular the simulation itself is run in the (BLAS) language of `gsl_matrix_complex` algebra.

A highly minimalistic, commented version of the TDHFT program is included with this report. Most of the features used for measuring the properties of the system (such as the position of the compression front) have been removed for brevity. There are three `.cpp` source files which may be compiled to produce corresponding `.exe` files. When compiling, it is necessary to link to the GSL installation. The parameters of the simulations must be changed within the source files themselves. Physical parameters are the basis dimension, d, electron number, N, shunt parameter, q, quasi-one-dimensionality parameter, ξ and a coupling constant proportional to e^2. It is further possible to change the resolution of the FFT, the number of iterations for both ground state convergence and time evolution, and the time step. The first program, `kernel.exe`, performs the FFT on the pair potential, storing the result in the file `kernel.dat` in the home directory. Next, `integrator.exe` forms libraries of the matrices Λ_{jk} and Π_{jk} respectively in the files `hartree.dat` and `exchange.dat`. The addresses, j, k of the matrices within these files are stored separately in `Ha_lookup.dat` and `Ex_lookup.dat`. Finally `simulator.exe` performs the simulation, printing the nth iteration in the sub-directory `/frames/` as `frame_n.png`. The current simulation method involves piping to Gnuplot. It is vital

that `simulator.cpp` be initialized before compiling so that the path to `gnuplot.exe` is specified in the file: if the program cannot call Gnuplot it will be unable to output data.

All plots which appear in this report were produced using Wolfram Mathematica 11.0.

References

[1] L. Calmels, A. Gold. Compressibility of the electron gas: Analytical results for width effects within the Hartree-Fock approximation. *Physical Review B*, 53 16, 1995.

[2] L. Salasnich, F. Toigo. Shell effects in the first sound velocity of an ultracold Fermi-gas. *Journal of Low Temperature Physics*, 150 3, 2008.

[3] E. Friedland. Radiation damage in metals. *Critical Reviews in Solid State and Materials Science*, 26 2 87-143, 2001.

[4] C. Race, D. Mason, M. Finnis, W. Foulkes, A. Horsfield, A. Sutton. The treatment of electronic excitations in atomistic models of radiation damage in metals. *Reports on Progress in Physics*, 73 11, 2010.

[5] P. Echenique, R. Nieminen, R. Ritchie. Density functional calculation of stopping power of an electron gas for slow ions. *Solid State Communications*, 37 779-781, 1981.

[6] P. Echenique, R. Ritchie. Spatial excitation patterns induced by swift ions in condensed matter. *Physical Review B*, 20 7, 1979.

[7] J. Pruneda, D. Sanchez-Portal, A. Arnau, J. Juaristi, E. Artacho. Electronic stopping power in LiF from first principles. *Physical Review Letters*, 99 235501, 2007.

[8] M. Ahsan Zeb, J. Kohanoff, D. Sanchez-Portal, A. Arnau, J. Juaristi, E. Artacho. Electronic stopping power in gold: the role of d electrons and the H/He anomaly. *Physical Review Letters*, 108 225504, 2012.

[9] L. D'Alessio, Y. Kafri, A. Polkovnikov, M. Rigol. From quantum chaos and eigenstate thermalization to statistical mechanics and thermodynamics. *Advances in Physics*, 65 239, 2016.

[10] L. Ye, X. Zheng, Y. Yan, M. Di Ventra. Thermodynamic meaning of local temperature of nonequilibrium open quantum systems. *Physical Review B*, 94 245105, 2016.

[11] C. Stafford. Local temperature of an interacting quantum system far from equilibrium. *Physical Review B*, 93 245403, 2016.

[12] F. Styer. Quantum revivals versus classical periodicity in the infinite square well. *American Journal of Physics*, 69 56, 2001.

[13] H. Gould. *Combinatorial identities, a standardized set of tables listing 500 binomial coefficient summations.* Published by the author, 1972.

[14] E. Henley, W. Thirring *Elementary quantum field theory.* McGraw-Hill Book Company, 1962.

[15] L. Schiff. *Quantum mechanics.* McGraw-Hill Book Company, 1988.

[16] L. Landau, E. Lifshitz *Quantum Mechanics (non-reativistic theory), Volume 3 of Course of Theoretical Physics.* Butterworth Heineman, 2003.

[17] N. Ashcroft, N. Mermin *Solid State Physics.* Holt, Rinehart and Winston, 1976.

[18] P. Kuchment *Floquet Theory for Partial Differential Equations.* Springer, 1993.